Cell Reports
Article

Cell PRESS
Open ACCESS

Loss of MEC-17 Leads to Microtubule Instability and Axonal Degeneration

Brent Neumann[1] and Massimo A. Hilliard[1,*]
[1]Queensland Brain Institute, The University of Queensland, Brisbane, QLD 4072, Australia
*Correspondence: m.hilliard@uq.edu.au
http://dx.doi.org/10.1016/j.celrep.2013.12.004

SUMMARY

Axonal degeneration arises as a consequence of neuronal injury and is a common hallmark of a number of neurodegenerative diseases. However, the genetic causes and the cellular mechanisms that trigger this process are still largely unknown. Based on forward genetic screening in *C. elegans*, we have identified the α-tubulin acetyltransferase gene *mec-17* as causing spontaneous, adult-onset, and progressive axonal degeneration. Loss of MEC-17 leads to microtubule instability, a reduction in mitochondrial number, and disrupted axonal transport, with altered distribution of both mitochondria and synaptic components. Furthermore, *mec-17*-mediated axonal degeneration occurs independently from its acetyltransferase domain; is enhanced by mutation of *coel-1*, a tubulin-associated molecule; and correlates with the animal's body length. This study therefore identifies a critical role for the conserved microtubule-associated protein MEC-17 in preserving axon integrity and preventing axonal degeneration.

INTRODUCTION

Maintenance of axonal structure is critical for neuronal function. Under normal conditions, the axon is maintained in a healthy state through a constant supply of materials via its attachment to the cell body. This connection is lost after nerve injury and becomes compromised in a number of neurodegenerative diseases, leading to degeneration of the axon (Coleman, 2005; Raff et al., 2002). Specific cellular mechanisms that have been linked to axonal degeneration include deficits in axonal transport, mitochondrial dysfunction, increase in intra-axonal calcium, and calcium-dependent cytoskeletal breakdown (Coleman, 2005; Hilliard, 2009; Wang et al., 2012). A major component of the cytoskeleton is formed by the microtubules, cylindrical structures assembled from chains of α- and β-tubulin heterodimers termed protofilaments (Desai and Mitchison, 1997). These highly dynamic structures are essential for many cellular functions, including intracellular transport and organelle positioning, as well as cell division and polarity (Westermann and Weber, 2003). Microtubules are subjected to a wide range of posttranslational modifications, including acetylation (Janke and Bulinski, 2011), the major site of which occurs on lysine 40 of α-tubulin inside the microtubule lumen (Nogales et al., 1998). Although it has largely been considered as a passive marker of stable microtubules (Hammond et al., 2008), several studies have postulated that acetylation of α-tubulin is required for efficient axonal transport, allowing greater binding and movement of motor proteins (Cai et al., 2009; d'Ydewalle et al., 2011; Dompierre et al., 2007; Hammond et al., 2010; Konishi and Setou, 2009; Reed et al., 2006). Loss or reduction in the levels of acetylated α-tubulin has also been associated with a number of pathological conditions, including familial dysautonomia and Alzheimer's, Huntington's, and Charcot-Marie-Tooth diseases (d'Ydewalle et al., 2011; Dompierre et al., 2007; Gardiner et al., 2007; Hempen and Brion, 1996).

Despite acetylation of K40 first being described in 1985 (L'Hernault and Rosenbaum, 1985), the identity of the α-tubulin acetyltransferase enzyme and the precise functional consequence of the modification remained unresolved until recently, when MEC-17/αTAT1 was identified as the acetylating enzyme conserved across all ciliated organisms (Akella et al., 2010; Shida et al., 2010). Significant insights into its function have now emerged, with two recent studies in *C. elegans* demonstrating that MEC-17 is critical for microtubule organization, stabilizing their number and length, and defining protofilament number (Cueva et al., 2012; Topalidou et al., 2012). Furthermore, Cueva et al. (2012) propose that K40 acetylation promotes the formation of stabilizing salt bridges between protofilaments, thereby creating structural supports within the microtubule lumen. In spite of the apparent importance of MEC-17, only a few morphological alterations have been linked to its loss. These include an increase in microtubule dynamics in *Tetrahymena* (Akella et al., 2010), a progressive loss of mechanosensory neuron function and minor neurite outgrowth defects in *C. elegans* (Topalidou et al., 2012; Zhang et al., 2002), and behavior consistent with neuromuscular defects in zebrafish (Akella et al., 2010). In *C. elegans*, MEC-17 is expressed solely in the six mechanosensory neurons (Zhang et al., 2002) and functions redundantly with its more broadly expressed paralog, ATAT-2 (Akella et al., 2010; Shida et al., 2010).

Here, we show that MEC-17 is critical for maintaining axonal structure, with mutations causing spontaneous, adult-onset,

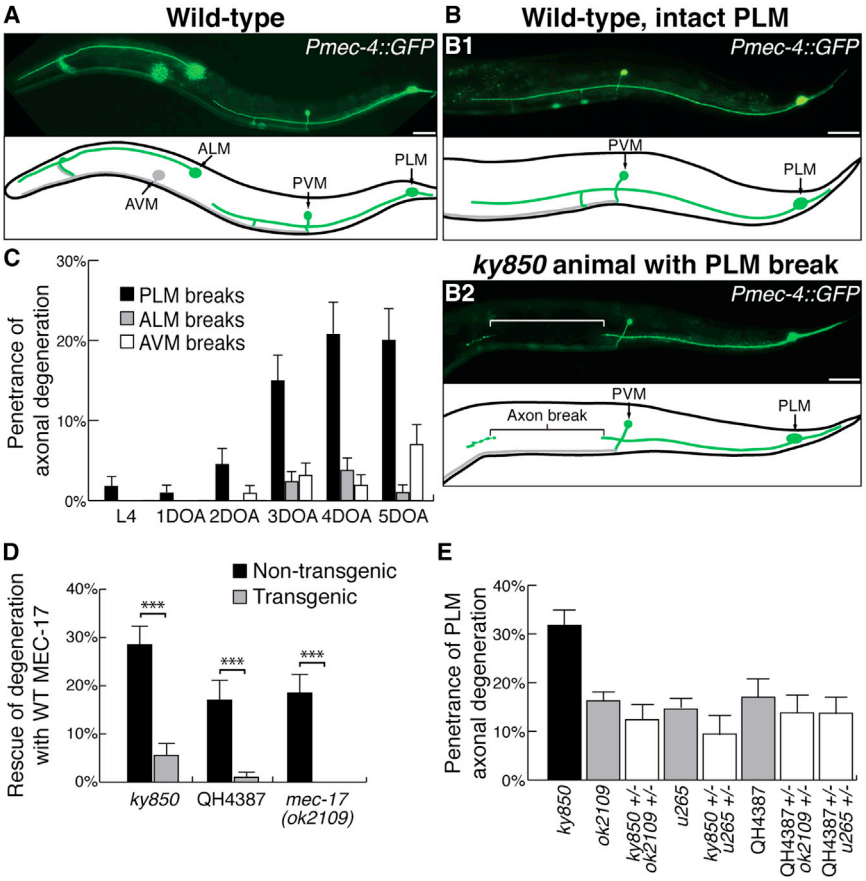

Figure 1. Identification and Mapping of the *ky850* Mutation

(A) Image and schematic of a wild-type *zdIs5*(*Pmec-4::GFP*) larval-stage four (L4) animal, illustrating the six mechanosensory neurons (PLML/R, PVM, ALML/R, and AVM). Anterior is left and ventral is down in this and all subsequent images.

(B) Image and schematic of a typical intact PLM neuron from a 3-day-old adult wild-type animal (B1) and that of a typical axon break (bracketed region) in a 3-day-old adult *ky850* mutant (B2).

(C) Axonal breaks quantified in *mec-17*(*ok2109*) animals of progressive ages. Similar results were obtained for *mec-17*(*u265*) animals (data not shown). DOA, day-old adult.

(D) Penetrance of axonal breaks in *ky850*, QH4387 (3× outcrossed *ky850*), and *mec-17*(*ok2109*) animals, carrying the *Pmec-4::mec-17* rescue transgene versus nontransgenic siblings.

(E) Penetrance of axonal degeneration in *ky850* (black bar) animals and the different *mec-17* alleles (gray bars). F1 cross progeny (white bars) were analyzed for phenotypic complementation.

The scale bars represent 25 μm; error bars represent SE of proportion; n ≥ 100 animals; ***p < 0.001.

and progressive axonal degeneration in *C. elegans*. This phenotype is independent of the role of MEC-17 in acetylating α-tubulin, as an enzymatically inactive version retains the ability to protect axons from degeneration. Loss of MEC-17 disrupts axonal transport, causing a decrease in the number and spatial arrangement of axonal mitochondria and an altered distribution of presynaptic loci. We find that MEC-17 functions in synergy with the microtubule-associated protein COEL-1 to stabilize microtubules and protect from axon fragility. Furthermore, our results establish that axonal degeneration can be strongly enhanced by elongation of the axonal shaft resulting from increased body length.

RESULTS

Isolation of the *ky850* Strain with Axonal Degeneration

To identify factors required for the maintenance of axonal structure, we performed forward genetic screens using a *C. elegans* strain expressing GFP in the six mechanosensory neurons (PLML/R, PVM, ALML/R, and AVM; Figure 1A). This wild-type strain, carrying the transgene *zdIs5(Pmec-4::GFP)*, effectively displays no axonal degeneration (Figure S1A). We visually screened for animals displaying spontaneous axonal degeneration and identified the recessive *ky850* mutation as presenting GFP interruptions (axonal breaks) in the PLM, ALM, and AVM axons (Figure 1B). Degeneration of the separated distal fragments occurred in a stereotypical Wallerian-like fashion, with thinning, beading, and fragmentation occurring over the 24–96 hr following the initial breaks, but did not lead to a "die-back" phenotype. The defect appeared selectively in adult animals (adult-onset), and the penetrance increased progressively with age, reaching a maximum of 45% in PLM (Figure S1B). *ky850* animals displayed a deficit in their response to gentle mechanical stimuli (light-touch assay) applied to either their head or tail, indicating that both the anterior and posterior mechanosensory circuits (mediated by ALMs/AVM and PLMs, respectively) were dysfunctional (Figure S1C). In addition to axonal degeneration, we observed axonal outgrowth defects in *ky850* animals that appeared during development and worsened with age (Figures S1D and S1E).

The *ky850* Mutation Is an Allele of *mec-17*

Several lines of evidence revealed that *ky850* is an allele of the α-tubulin acetyltransferase gene *mec-17*. First, direct mapping from whole-genome sequencing data (Zuryn et al., 2010) revealed a strong peak on chromosome IV at the precise location of *mec-17* (Figure S1F), and we identified a C-T transition at nucleotide position 79 of the gene, resulting in the introduction of a stop codon in the encoded protein, truncating MEC-17 from 262 amino acids to 26 (Figure S1G). Second, cell-autonomous expression of wild-type MEC-17 in the mechanosensory neurons (using a *Pmec-4::mec-17* transgene) provided strong rescue of the degenerative phenotype (Figure 1D). Third, two other alleles of *mec-17* (*ok2109* and *u265*; Figure S1G) also presented with progressive, adult-onset axonal breaks in the

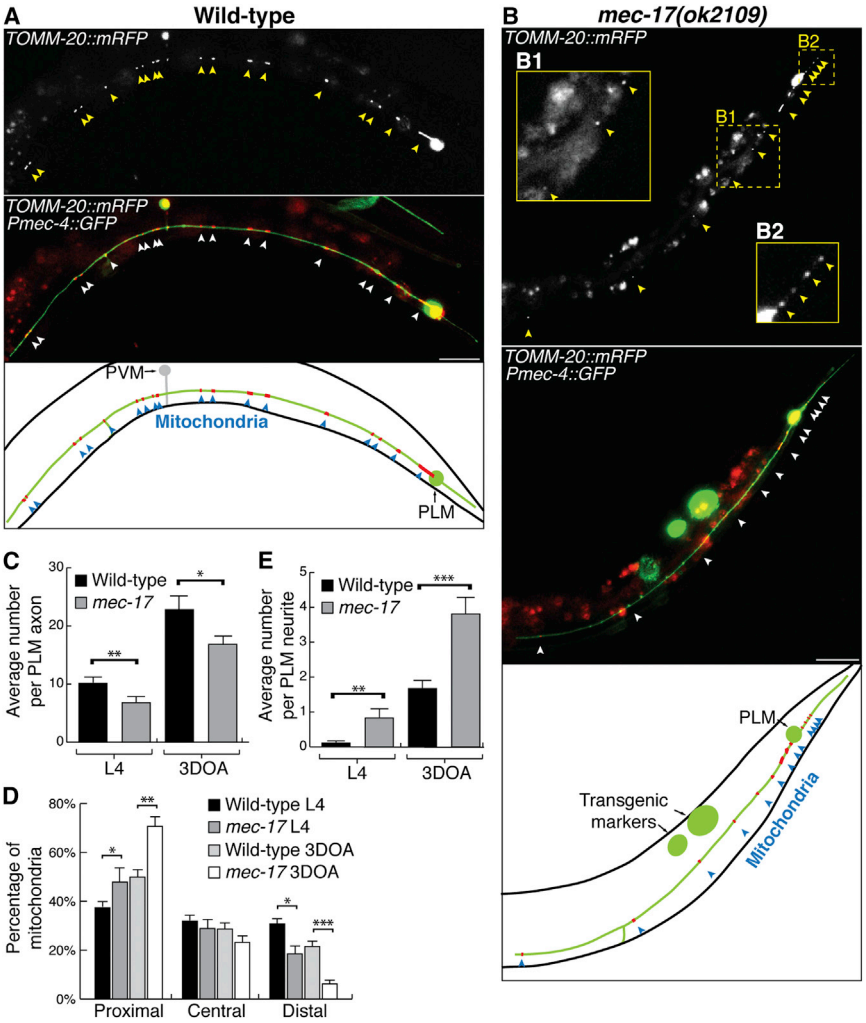

Figure 2. *mec-17* Mutants Display a Reduction in Axonal Mitochondria and a Clustering toward the Cell Body

(A and B) Image and schematic of mitochondria in PLM in both wild-type (A) and *mec-17*(*ok2109*) (B) 3-day-old adults. Mitochondria (arrowheads) were visualized with the *vdEx484*[*Pmec-4::tomm-20::mRFP*] transgene. (B1 and B2) Magnified view of the corresponding regions in the *mec-17* mutant animal to highlight faint mitochondria.

(C) Average number of mitochondria in PLM in wild-type and *mec-17*(*ok2109*) animals.

(D) Quantification of mitochondria in proximal (closest third to the cell body), central (middle third), and distal (final third) regions of the PLM axon in L4 and 3-day-old adults.

(E) Average number of mitochondria in the PLM posterior neurite in wild-type and *mec-17*(*ok2109*) animals.

The scale bars represent 25 μm; the error bars represent SEM; *p < 0.05; **p < 0.01; ***p < 0.001; n ≥ 26 animals.

mechanosensory neurons (Figure 1C). However, although the axon breaks were morphologically identical, the penetrance of degeneration in these strains was lower than in animals with the *ky850* mutation (21% compared to 45% in 5-day-old adults). This discrepancy is likely due to a background effect of additional mutations in the *ky850* strain, as outcrossing *ky850* reduced the penetrance of axonal degeneration to levels similar to those in *mec-17*(*ok2109*) animals (Figures 1D and 1E). Importantly, cell-autonomous expression of wild-type MEC-17 in either this outcrossed *ky850* strain (QH4387) or in the *mec-17*(*ok2109*) strain strongly rescued the degeneration observed in the PLM axon (Figure 1D). As previously described (Topalidou et al., 2012), the two other *mec-17* alleles displayed outgrowth defects in PLM and ALM, which were similar to those of *ky850* mutants, but again to a lower penetrance (Figure S1E). Finally, as we found all three alleles of *mec-17* (*ky850*, *ok2109*, and *u265*) to be recessive (no axonal degeneration in heterozygous animals; n > 100), we conducted complementation analyses of *ky850* or the outcrossed *ky850* strain (QH4387) with *ok2109* and *u265*, which revealed noncomplementation (Figure 1E), thereby confirming that the three mutations are alleles of the same gene.

Loss of *mec-17* Leads to Disruption of Mitochondria and Axonal Transport

To characterize the intra-axonal mechanisms disrupted by loss of MEC-17 function, we first analyzed mitochondria using a fluorescently tagged version of the translocase of outer mitochondrial membrane 20 protein (Kanaji et al., 2000; Figure 2A). The average number of mitochondria in *mec-17* (*ok2109*) animals was reduced compared to wild-type at both the L4 and adult stages (Figures 2A–2C). Furthermore, *mec-17*(*ok2109*) animals displayed a striking disruption in the localization of their mitochondria. Wild-type animals presented a relatively even distribution of mitochondria in the PLM axon in the L4 stage and a slightly skewed distribution toward the cell body in adulthood (Figure 2D). In contrast, *mec-17*(*ok2109*) animals had a skewed distribution of mitochondria at the L4 stage, with a reduced number of mitochondria in the distal segment. This defect was severely enhanced in adult animals, with the distal segment becoming largely devoid of mitochondria (Figures 2B and 2D). Interestingly, it was in these distal regions with reduced mitochondrial number that we observed the majority of the axonal breaks. In addition, we found that *mec-17*(*ok2109*) animals had a large increase in the number of mitochondria localized in the posterior PLM neurite (Figure 2E), corresponding to the additional outgrowth defects observed in *mec-17* mutants. We also observed similar mitochondrial defects in ALM neurites (Figures S2A–S2C). Taken together, these results uncover a critical role of MEC-17 in regulating the number and localization of mitochondria in the mechanosensory neurons.

A possible explanation for the mitochondrial defects is a disruption in axonal transport. We analyzed a fluorescently

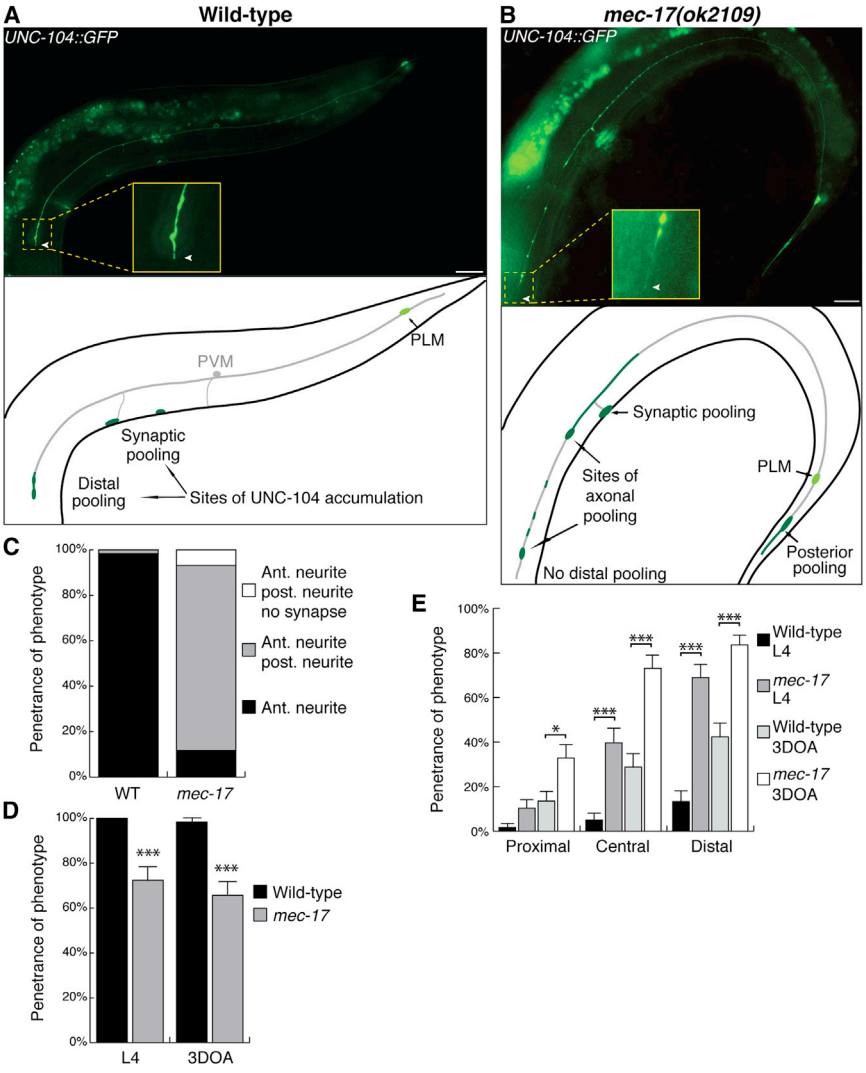

Figure 3. *mec-17* Animals Display Aberrant Axonal Transport

(A and B) Image and schematic of UNC-104/kinesin-3 in PLM of wild-type (A) and *mec-17*(*ok2109*) (B) 3-day-old adult animals used to monitor axonal transport. UNC-104 was visualized using the *jsIs1111*[*Pmec-4::unc-104::GFP*] transgene. Insets show a magnified view of the distal axon tips. Arrowheads point to the distal tip of the PLM axon. The scale bars represent 25 μm.

(C) Quantification of UNC-104::GFP localization in PLM in wild-type and *mec-17*(*ok2109*) animals. Anterior neurite defined as per image shown in (A), with anterior localization and accumulation at presynaptic sites. Gray bars indicate additional localization in the PLM posterior neurite. White bars designate localization in both the anterior and posterior neurites with no presynaptic accumulation.

(D) Comparison of the number of animals displaying UNC-104::GFP pooling at the distal end of the PLM axon.

(E) Accumulation of UNC-104::GFP measured in different regions along the PLM axon in wild-type and *mec-17*(*ok2109*) animals at the L4 stage and in 3-day-old adults. This analysis excludes pooling at the distal tip.

The error bars represent SE of proportion; $^{*}p < 0.05$; $^{***}p < 0.001$; $n \geq 51$ animals.

tagged version of UNC-104/kinesin-3 (Kumar et al., 2010), one of the main motor molecules responsible for transport of synaptic vesicles to presynaptic loci (Hall and Hedgecock, 1991). Wild-type animals exhibited a consistent distribution of fluorescence in PLM, with a smooth increase in expression along the axon in a proximal-to-distal fashion, and pooling at the distal end and at presynaptic sites (Figure 3A). By comparison, the vast majority of *mec-17*(*ok2109*) mutant animals displayed a bipolar distribution, with strong expression also observed in the posterior neurite (Figures 3B and 3C), and approximately 7% of animals completely lacked expression of UNC-104 at the presynaptic loci of PLM (Figure 3C). Furthermore, more than 25% of animals lacked accumulation at the distal end of the axon (Figure 3D) and instead displayed accumulation of bright puncta along more proximal sections of the axon (Figure 3E), indicative of disrupted axonal transport. To correlate these findings with localization of presynaptic components, we studied the distribution of the synaptic vesicle-associated small guanosine triphosphatase, RAB-3 (Nonet et al., 1997). Expression of RAB-3 in wild-type animals was strongly localized to the presynaptic terminals and only weakly within the cell body and proximal anterior axon (Figure 4A). On the contrary, 24% of *mec-17*(*ok2109*) mutant animals completely lacked expression of RAB-3 at the presynaptic sites of PLM (Figure 4C). Similar to the distribution of UNC-104, we also observed bipolar distribution of RAB-3 in *mec-17*(*ok2109*) animals, with clusters visible in the ends of the posterior neurite (Figures 4B and 4C). Similar deficits in the localization of UNC-104 and RAB-3 were observed in ALM neurons of *mec-17* mutants (Figures S2D and S2E).

Collectively, these findings suggest that, in the absence of MEC-17, axonal transport is defective, and as a result, the localization of presynaptic components and the number and distribution of mitochondria are disrupted, culminating in degeneration of the axon.

MEC-17-Mediated Acetylation of MEC-12 Is Not Required for Axonal Maintenance

MEC-17 has been demonstrated to function redundantly with its paralog, ATAT-2, in the acetylation of MEC-12/α-tubulin (Akella et al., 2010; Shida et al., 2010). To determine if ATAT-2 is also required in the maintenance of axonal structure, we analyzed *atat-2*(*ok2415*) animals, which have a deletion eliminating almost 60% of the *atat-2* transcript. Single mutants displayed no degenerative phenotype in the mechanosensory neurons, and double mutants with *mec-17* were not different from *mec-17* single

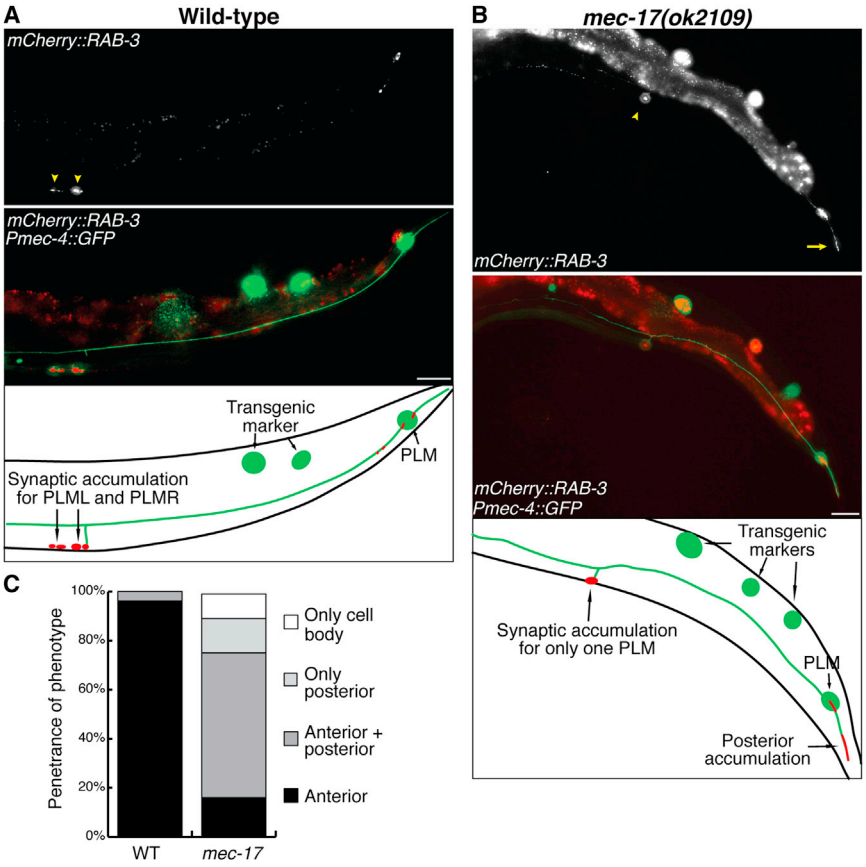

Figure 4. *mec-17* Animals Display Aberrant Localization of Presynaptic Components

(A and B) Image and schematic of PLM presynaptic loci in wild-type (A) and *mec-17*(*ok2109*) (B) 3-day-old adult animals visualized using the *vdEx262*[*Pmec-4::mCherry::rab-3*] transgene. Arrowheads point to presynaptic sites; arrow points to accumulation in the posterior neurite. The scale bars represent 25 μm.

(C) Localization of mCherry::RAB-3 analyzed in wild-type and *mec-17*(*ok2109*) animals. Anterior refers to localization in the anterior neurite (as in A); posterior refers to localization in the posterior neurite (as in B). n ≥ 52 animals.

mutants (Figure S3A), demonstrating that ATAT-2 does not function in axonal maintenance in these neurons. Next, to determine if the acetyltransferase domain of MEC-17 is needed for axonal maintenance, we generated a mutant version (MEC-17 [D144N]) lacking the ability to acetylate MEC-12/α-tubulin (Shida et al., 2010; Topalidou et al., 2012) and introduced it selectively in the mechanosensory neurons of *mec-17* mutant animals. As shown in Figure 5A, this version of MEC-17 could still rescue axonal breakage. Moreover, this acetyltransferase-dead version of MEC-17 could also completely rescue the mitochondrial distribution defect observed in *mec-17*(*ok2019*) mutant animals (Figures 5B and S3B), demonstrating that the acetyltransferase domain is not required for MEC-17 to prevent axonal degeneration. To determine whether MEC-12/α-tubulin functions in the *mec-17*-mediated degenerative phenotype, we studied animals carrying mutations in the *mec-12* gene. Two different alleles of *mec-12* (either *u63* or *u241*; Figure S3C) generated a highly penetrant, largely adult-onset, and severe degenerative phenotype in all six mechanosensory neurons (Figures 5C and S3E–S3G). Axonal degeneration of PLM in the double mutants with *mec-17* showed an allele-dependent effect (increased degeneration with *u63* and decreased with the dominant allele *u241*) confirming the functional interaction between MEC-17 and MEC-12. Interestingly, loss of function of the other microtubule subunit, MEC-7/β-tubulin, also caused severe axonal degeneration in the mechanosensory neurons (Figures 5D, S3D, and S3H) that was exacerbated by mutation in *mec-17*, again indicating functional synergy. Furthermore, we found similar defects in the distribution of mitochondria in *mec-12* and *mec-7* mutant animals as those in *mec-17* mutants (Figures S3I and S3J). To further investigate the role of the MEC-17 acetyltransferase domain in axonal degeneration, we analyzed a mutant version of MEC-12 that could not be acetylated at the K40 site (K40R; Akella et al., 2010). As shown in Figure 5E, MEC-12(K40R) could rescue the degeneration observed in *mec-12*(*e1607*) animals to similar levels as wild-type (WT) MEC-12. Finally, we found that MEC-12(K40R) animals display mitochondria along the PLM axon as per WT animals (Figures 5B and S3B). Together, these data conclusively demonstrate that acetylation of MEC-12 is redundant for MEC-17's role in maintaining axonal structure and reveal a critical role for each microtubule subunit, MEC-12/α-tubulin and MEC-7/β-tubulin, in maintaining axonal integrity after development.

Mutation of *mec-17* Leads to Microtubule Instability

Although the acetylation activity of MEC-17 was not required for its function in axonal maintenance, our results with MEC-12 and MEC-7 suggested that loss of *mec-17* might negatively affect microtubule stability. To directly visualize microtubule dynamics in PLM, we analyzed a GFP-tagged version of end-binding protein 2 (EBP-2), a marker of plus-end-growing microtubules (Srayko et al., 2005). As the majority of EBP-2::GFP "comets" (growing microtubules) have previously been demonstrated to occur close to the cell body under resting conditions (Ghosh-Roy et al., 2012), we used spinning-disk confocal microscopy and kymographs to analyze the initial 25 μm of the PLM axon (Figures 6A and 6B; Movie S1). Remarkably, as shown in Figure 6C and Movie S2, animals carrying the *mec-17*(*ok2109*) mutation displayed a 2-fold increase in the number of growing microtubules compared to WT animals. Moreover, whereas the vast majority of microtubules grew in the anterograde direction in WT animals, *mec-17*(*ok2109*) mutants presented a significantly higher proportion of EBP-2::GFP comets moving in the

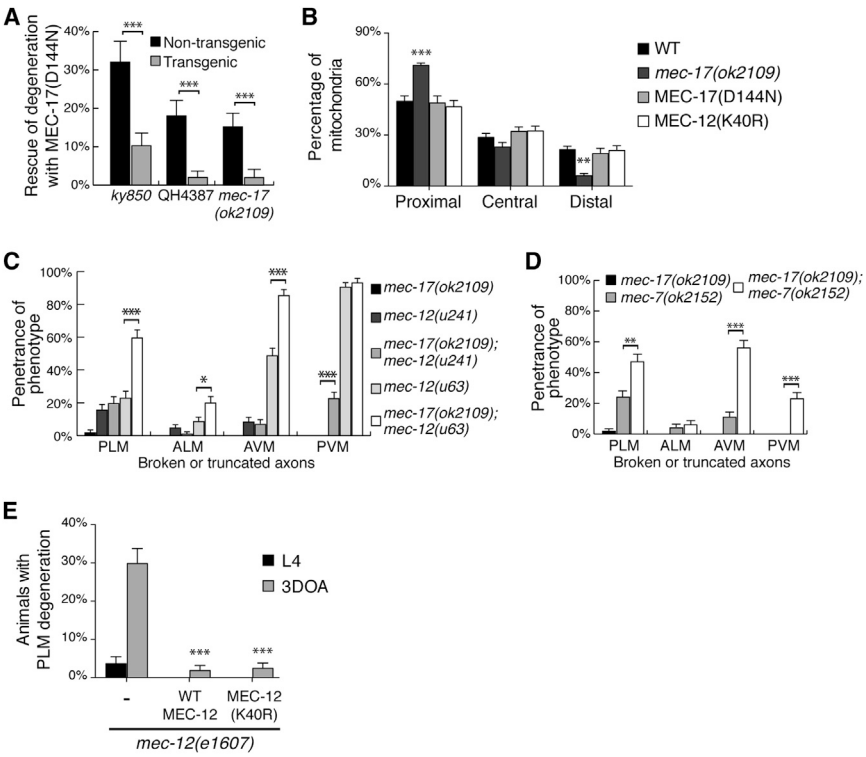

Figure 5. MEC-17 Acetyltransferase Activity Is Not Required for Axonal Maintenance

(A) Expression of MEC-17 lacking acetyltransferase activity from the *Pmec-4::mec-17*(*D144N*) transgene rescues the axonal degeneration phenotype in *ky850*, QH4387 (3× outcrossed *ky850*), and *mec-17*(*ok2109*) animals, compared to their nontransgenic siblings.

(B) Expression of the *Pmec-4::mec-17*(*D144N*) transgene rescues the mitochondrial distribution defect found in 3-day-old adult *mec-17*(*ok2109*) animals, restoring their localization to the WT pattern. MEC-12(K40R) (lacking acetylation residue) animals display a normal distribution of mitochondria.

(C) Quantification of axonal degeneration (L4 stage) in animals carrying single and double mutations in MEC-17 and MEC-12/α-tubulin.

(D) Comparison of axonal degeneration (L4 stage) in *mec-17* and *mec-7* (encoding β-tubulin) single and double mutants.

(E) Rescue of PLM axonal degeneration in *mec-12*(*e1607*) animals with WT MEC-12 or with the MEC-12(K40R) mutated version.

The error bars represent SE of proportion (A and C–E) and SE (B); *$p < 0.05$; **$p < 0.01$; ***$p < 0.001$; n ≥ 100 animals (A and C–E) and ≥24 animals (B).

retrograde direction (Figure 6D). Whereas no changes in microtubule track length, growth duration, or catastrophe frequency were observed, the velocity of microtubule growth was significantly reduced in adult *mec-17*(*ok2109*) animals (Figures S4A–S4D). These data indicate that loss of MEC-17 function leads to a destabilization of the microtubule network, causing a greater frequency of microtubule growth and disrupting microtubule polarity within the axon.

We extended our analyses of microtubule stability by treating animals with microtubule-stabilizing (paclitaxel) or -destabilizing (colchicine) compounds (Fojo, 2008). Treatment of *mec-17* mutants with paclitaxel led to a more than 6-fold decrease in the penetrance of PLM axonal degeneration (Figures 6E, S4E, S4G, and S4H). Next, using a concentration that had no effect on wild-type animals, we treated *mec-17* mutants with colchicine and found a more than 5-fold increase in axonal degeneration (Figures 6E and S4F–S4H). Interestingly, the mitochondrial distribution defects observed in *mec*-17 mutants (Figure 2D) were rescued with paclitaxel treatment and exacerbated by colchicine (Figures S4I and S4J), supporting a correlation between mitochondrial mislocalization and axonal degeneration.

We further tested the effect of *mec-17* mutation on axonal stability by investigating the genetic interaction between *mec-17* and *coel-1*. COEL-1 is homologous to the tubulin-folding cofactor E-like molecule, which is involved in tubulin stability (Bartolini et al., 2005). Mutation of *coel-1* by itself was not sufficient to induce a degenerative phenotype in the mechanosensory neurons and did not present an altered distribution of mitochondria (Figures 6F and S5A–S5C). However, when combined with mutation of *mec-17*, we observed a 2-fold enhancement in the penetrance of axonal breaks in both PLM and AVM (Figure 6F), demonstrating a genetic interaction between the two genes.

Finally, to determine if MEC-17-induced axon degeneration was due to an acquired axonal fragility, we investigated the effect of physical tension from the animal's movement on axonal structure. We analyzed *mec-17* mutant animals paralyzed by RNAi against *unc-54*, the gene encoding the major *C. elegans* myosin heavy chain (MacLeod et al., 1977). Paralysis of *mec-17* mutants induced a strong suppression of axonal degeneration (Figure 6G), indicating that the mechanical stress applied to the axons by simple body movement was sufficient to cause spontaneous breaks. These results support a model in which MEC-17 acts to stabilize the microtubules so as to prevent the axon becoming vulnerable to physical strain.

Body Length Correlates with Axonal Degeneration

In outcrossing the *ky850* mutant animals, we serendipitously identified a mutant animal with an elongated body (LONg phenotype), which displayed a significant increase in the number of axonal breaks. We mapped and cloned this spontaneous mutation and found it to be an allele (*vd037*) of the gene *lon-3* (encoding for a cuticle collagen; Nyström et al., 2002). A second known *lon-3* allele (*e2175*) was also able to significantly enhance the axonal degeneration phenotype of *mec-17* mutants (Figure 7). To test if the enhancement of axonal degeneration was caused by the specific disruption of *lon-3*, or more generically by the longer body shape, we analyzed other mutant strains displaying similar elongated morphology (Figures 7 and S6A). We studied another two conserved genes from the transforming growth

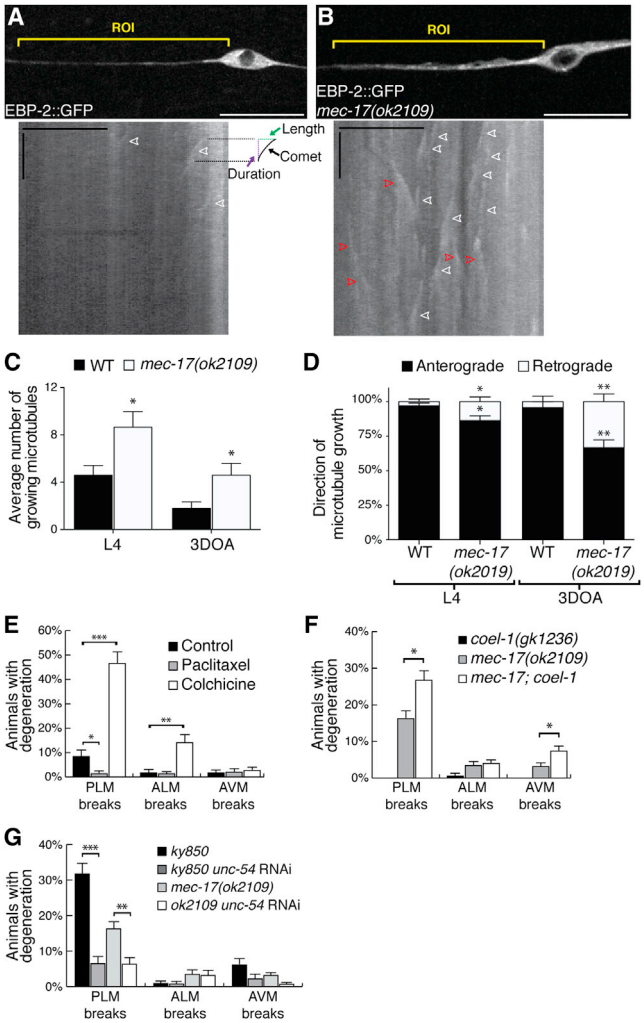

Figure 6. Loss of *mec-17* Causes Microtubule Instability and Axon Fragility

(A) A representative image of PLM in a L4 WT animal carrying the *Pmec-4::ebp-2::GFP* transgene that highlights the 25 μm region of interest (ROI) analyzed in the kymograph shown below the image. Schematic adjacent to kymograph illustrates how comets were traced and measured for growth length and duration. White arrows point to comets growing in the anterograde direction.

(B) Representative image of EBP-2::GFP expressed in PLM of a mutant *mec-17*(*ok2109*) L4 animal, with an increased number of microtubule comets, as evident in the kymograph below the image. White arrows point to comets growing in the anterograde direction; red arrows to those in the retrograde direction. For both (A) and (B), the scale bar in the images represents 10 μm; scale bars in the kymographs represent 10 μm for the x axis, and 10 s for the y axis.

(C) Mutation of *mec-17*(*ok2109*) causes a significant increase in the number of EBP-2::GFP comets compared to WT in L4 and 3-day-old adult animals. n = 15 animals for WT, and n ≥ 11 for *mec-17*(*ok2109*).

(D) EBP-2::GFP comets grow significantly more in the retrograde direction in both L4 and 3-day-old adult *mec-17*(*ok2109*) mutants compared to WT. n ≥ 25 comets for WT and n ≥ 69 for *mec-17*(*ok2109*).

(E) *mec-17*(*ok2109*) animals were grown on control agar containing 1% DMSO or agar containing either 1 μM paclitaxel (microtubule stabilizer) or 0.1 mM colchicine (microtubule destabilizer) and scored as 2-day-old adults.

(F) Penetrance of axonal degeneration in 3-day-old adult *coel-1*(*gk1236*), *mec-17*(*ok2109*), or *coel-1; mec-17* double mutants.

(G) Animals carrying the *ky850* or *mec-17*(*ok2109*) mutations were paralyzed by microinjection of *unc-54* dsRNA and the penetrance of breaks compared to that in nontreated animals.

The error bars represent SE (C and D) and SE of proportion (E–G); *p < 0.05; **p < 0.01; ***p < 0.001; n ≥ 100 animals for (E–G).

factor β (TGF-β)-like-signaling pathway, *lon-1* (a pathogenesis-related protein; Morita et al., 2002) and *lon-2* (a glypican; Gumienny et al., 2007), as well as the TGF-β-signaling independent gene, *lon-8* (Soete et al., 2007). Mutations in these genes caused a mild axonal degenerative phenotype (Figure S6B). However, when combined with the *mec-17*(*ok2109*) mutation, all four genes caused a remarkable increase in axonal degeneration (Figure 7).

We postulated that this enhancement in degeneration could be due to the increased demands placed upon the cell body in order to maintain a significantly longer axon. To test this hypothesis, we analyzed shorter animals to determine if axonal degeneration was suppressed. As previously described, mutation of the genes *sma-3* (a receptor-regulated Smad), *sma-4* (a Smad protein), *sma-6* (a TGF-β-like type I receptor), and *dbl-1* (a bone-morphogenic-protein-like TGF-β-signaling molecule) results in reduced body size (Krishna et al., 1999; Savage et al., 1996; Savage-Dunn et al., 2000; Suzuki et al., 1999; Figures 7 and S6A). We found no degenerative phenotype in single mutants (n > 100 animals analyzed), and all four mutations significantly suppressed the degenerative phenotype in *mec-17*(*ok2109*) mutants (Figure 7). To ensure that these modulating effects were not due to underlying differences in the developmental status of the long versus short animals, we performed lifespan experiments. We found no correlation between body morphology and lifespan (Figures S6C and S6D) and extended these findings by analyzing degeneration in animals mutant for *daf-2*, a receptor tyrosine kinase molecule that when mutated causes a doubling in the lifespan of *C. elegans* (Kenyon et al., 1993). The penetrance of axonal degeneration in *mec-17*; *daf-2* double mutants was not significantly different from that in *mec-17* single-mutant animals (Figure S6E). These results reveal an underlying role of the animal's body morphology in the capacity of the neuron to preserve axonal structure over time.

DISCUSSION

The axon frequently extends many times the length of the cell body. As such, maintenance of the axonal structure over an organism's lifetime imposes considerable strain and requires effective transport of organelles, specific molecules, and trophic factors along the axonal shaft. In particular, cumulative evidence supports a critical role for mitochondrial transport and function in axonal maintenance (Court and Coleman, 2012). Furthermore, maintenance of axonal structure is dependent on an intact microtubule network that is not only vital for providing structural support but also allows the movement of motor proteins, which rely on the microtubules for axonal trafficking (Falnikar and Baas, 2009). Our results identify the crucial contribution of MEC-17 in preserving axonal structure and suggest a model in which

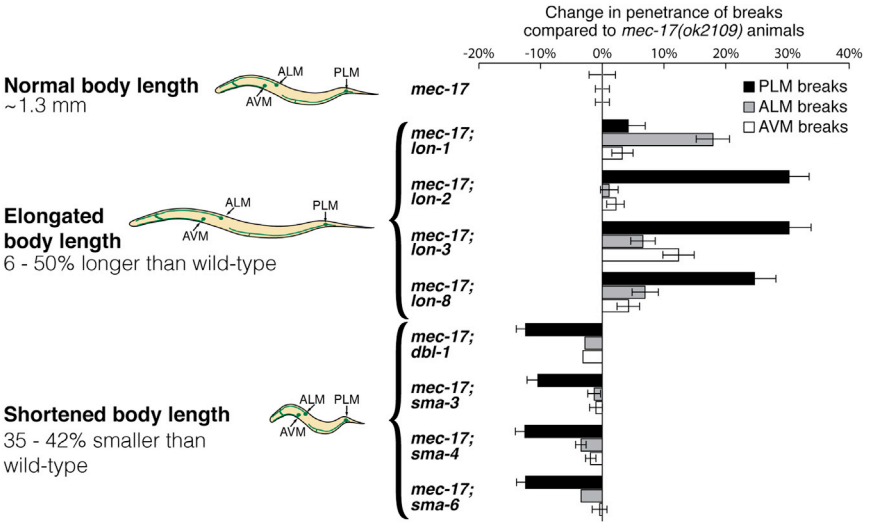

Figure 7. Axon Degeneration Is Modulated by Body Morphology in *mec-17* Mutants

Schematics show percentage increase or decrease in body length of 3-day-old adults caused by mutations in different genes. Bar graph represents the increase or decrease in the penetrance of degeneration in *mec-17*(*ok2109*) mutants when combined with body-elongating mutations (*lon-1*(*e185*), *lon-2*(*e678*), *lon-3*(*e2175*), *lon-8*(*hu187*)) or shortening mutations (*dbl-1*(*nk3*), *sma-3*(*e491*), *sma-4*(*e729*), *sma-6*(*e1482*)).

The error bars represent SE of proportion; n ≥ 160 animals.

MEC-17 stabilizes the microtubules to allow efficient binding and movement of motor proteins, thus permitting correct transport of mitochondria and other essential cargo throughout the axon.

The disrupted localization of UNC-104/kinesin-3, combined with mislocalization of RAB-3 and mitochondria, suggest a role for MEC-17 in maintaining efficient axonal transport. Mitochondria are critical for axonal health, carrying out essential functions in generating adenosine triphosphate, buffering intracellular Ca^{2+} and reactive oxygen species, and synthesizing various cellular components (Court and Coleman, 2012; Martin, 2012). Efficient, long-distance transport of mitochondria relies upon kinesin and dynein motor proteins, as well as the microtubule tracks that guide them (Hollenbeck, 1996). MEC-17 is critical for microtubule architecture (Cueva et al., 2012; Topalidou et al., 2012), and here we show that, in the absence of *mec-17*, microtubules are destabilized, axonal transport disrupted, and axon segments furthest from the cell body become largely devoid of mitochondria. The vast majority of axon breaks we observed occurred within these mitochondria-barren regions, suggesting that MEC-17 is required to keep a consistent distribution and number of mitochondria for proper neuronal maintenance. However, it is equally plausible that loss of axonal stability in the absence of MEC-17 prevents the movement of mitochondria out of the distal axon regions, leading to their degradation and thus a reduction in their numbers.

Our data support a role for MEC-17 in stabilizing the microtubules. We find a strong enhancement of microtubule dynamics in animals mutant for *mec-17*, suggesting that loss of MEC-17 causes instability of the microtubule network, leading to excessive microtubule turnover and more microtubules entering the growth phase in compensation. Furthermore, axonal degeneration and mitochondrial-distribution defects induced by the absence of *mec-17* could be strongly suppressed with a microtubule-stabilizing drug and significantly enhanced by mild destabilization. In addition, we found qualitatively similar, albeit more severe, axonal degeneration phenotypes in animals lacking MEC-12/α-tubulin and MEC-7/β-tubulin, and a genetic interaction of *mec-17* with mutations in either of these tubulins. Our genetic analysis defines a synergic role of MEC-17 with the tubulin-folding cofactor-E-like molecule COEL-1, a molecule related to a murine model of motor neuron disease (progressive motor neuronopathy) characterized by progressive axonal degeneration (Bommel et al., 2002).

Previous studies have shown that acetylation of α-tubulin does not affect microtubule stability and that the acetyltransferase domain of MEC-17 is not required for correct neurite outgrowth or neuronal function (Perdiz et al., 2011; Cueva et al., 2012; Topalidou et al., 2012). However, the enzymatic activity of MEC-17 is required for regulating the organization and number of microtubules and the protofilaments within them. Two recent publications have made the surprising discovery that the microtubules of fibroblasts with knockdown of *mec-17*/*αTAT1* expression, or derived from MEC-17/αTAT1-null mice, show resistance to the depolymerizing agent nocodazole (Kalebic et al., 2013a, b). These results add to the growing intrigue of the MEC-17 molecule and may point toward cell-specific effects on microtubule stability, with the molecule promoting stability in the nervous system but acting to destabilize the microtubules network in order to promote cytoskeletal rearrangements and cell motility in other tissues. Our data showing that MEC-17 functions independently from its acetyltransferase domain in preventing axonal degeneration support the notion of enzymatic-dependent and -independent functions, with MEC-17 binding within the microtubule lumen and likely acting as a structural support to modulate microtubule organization (Cueva et al., 2012; Topalidou et al., 2012). Whereas at present we cannot exclude the existence of other domains capable of still-unidentified enzymatic activities, our study reveals a critical role for MEC-17 in modulating microtubule stability and protecting from axonal degeneration.

EXPERIMENTAL PROCEDURES

Strains

Strains were cultured under standard conditions (Brenner, 1974), and all experiments were performed at room temperature (22°C). The wild-type N2 Bristol and CB4856 Hawaiian isolates and the following mutations were used: LGII: *sma-6*(*e1482*); LGIII: *daf-2*(*e1370*), *mec-12*(*u63*), *mec-12*(*u241*), *mec-12*(*e1607*), *sma-4*(*e729*), *lon-1*(*e185*), *sma-3*(*e491*); LGIV: *mec-17*(*ok2109*), *mec-17*(*u265*), *mec-17*(*ky850*); LGV: *dbl-1*(*nk3*), *lon-3*(*vd037*), *lon-3*(*e2175*),

lon-8(*hu187*); and LGX: *coel-1*(*gk1236*), *lon-2*(*e678*), *atat-2*(*ok2415*), *mec-7*(*ok2152*).

Transgenes used were: *zdIs5(Pmec-4::GFP)*, *vdEx267/vdEx539/vdEx546 (Pmec-4::mec-17* [10 ng/μl]; *Plad-2::mCherry)*, *vdEx484(Pmec-4::tomm-20::mRFP* [0.5ng/μl]; *Punc-122::GFP* [25 ng/μl]), *jsIs1111(Pmec-4::unc-104::GFP*; a gift from Sandhya Koushika), *vdEx262(Pmec-4::mCherry::rab-3* [0.5 ng/μl]; *Punc-122::GFP* [25 ng/μl]), *vdEx411/vdEx543/vdEx548 (Pmec-4::mec-17[D144N]* [10 ng/μl]; *Podr-1::dsRed* [30 ng/μl]), *juEx2843(Pmec-4::EBP-2::GFP*; a gift from Anindya Ghosh-Roy and Andrew Chisholm); *ekSi1(Pmec-12::mec-12::3′ UTR mec-12)* II; *ekSi3(Pmec-12::mec-12 [K40R]::3′ UTR mec-12)* II (both were gifts from Jacek Gaertig).

Isolation of Mutants and Genetic Mapping

Animals of genotype *zdIs5; sir-2.1*(*ok434*) were mutagenized using 50 mM ethyl methanesulfonate (Sigma) for 4 hr. The *ky850* mutation was isolated from a clonal F2 progeny screen, and the *sir-2.1* mutation was found not to influence the phenotype. These animals were crossed to wild-type CB4856 males, and single nucleotide polymorphism (SNP) mapping was performed using 11 previously described SNPs per chromosome (Davis et al., 2005; Wicks et al., 2001), which mapped the mutation to a central region on chromosome IV. The *ky850* isolate was backcrossed 10× with the parental *zdIs5; sir-2.1* line, before whole-genome sequencing was conducted on each (Australian Genome Research Facility), reaching a mean depth of 16.6–16.9.

The *lon-3*(*vd037*) allele consists of a 3,525 bp deletion spanning from the left flank sequence 5′-ttgccagagagagaaagttgacaaaacaat-3′ to the right flank sequence 5′-tcctgttgggcaagtattctccacagtaca-3′ and an insertion of 12 bp (gggcaagtattc). Genotyping was performed using the following primers: outer left 5′-agagcacaatgacactctttcc-3′; outer right 5′-agatatccattgtcgttcttcccc-3′; inner left 5′-aagcaaatgaccgatcgacc-3′; and inner right 5′-tcacgtatgttgacaaata tcagg-3′.

Molecular Biology

Standard molecular biology techniques were used. The *Pmec-4::mec-17* plasmid was generated by replacing the GFP sequence from the *Pmec-4::GFP* plasmid with an XmaI/AgeI full-length genomic *mec-17* sequence (amplified from N2 genomic DNA using 5′-atgcaagtcgacgccgacctcc-3′ and 5′-tcaccacaatggcttgctcgacag-3′ primers). *Pmec-4::tomm-20::mRFP* was created by replacing the *myo-3* promoter from *Pmyo-3::tomm-20::mRFP* (Ichishita et al., 2008) with an HindIII/XbaI *Pmec-4* sequence (amplified from *Pmec-4::GFP* using 5′-aagcttcaatacaagctcaa-3′ and 5′-tctataacttgatagc gata-3′ primers). The *Pmec-4::mCherry::rab-3* plasmid was created by replacing GFP in *Pmec-4::GFP* with mCherry and subsequently inserting a FseI/AscI *rab-3* coding sequence downstream from mCherry. The *rab-3* sequence was amplified from the *Prab3::eGFP::RAB3::rim-3* plasmid (a gift from Michael Nonet, Washington University in St. Louis; using 5′-gctggcggacaacctcaagg-3′ and 5′-ttagcaattgcattgctgttgagc-3′ primers). QuikChange Site Directed Mutagenesis (Agilent Technologies) was used to create the *Pmec-4::mec-17*(*D144N*) plasmid, with *Pmec-4::mec-17* used as the template and the following primers: sense: 5′- gaaccttatcaattggctcttaataatccatcagtcactcttc-3′ and antisense: 5′-gaagagtgactgatggattattaagagccaattgataaggttc-3′.

To induce paralysis, P0 animals were microinjected with double-stranded RNA (dsRNA) against *unc-54*, transcribed with a MEGAscript T7 In Vitro Transcription Kit (Life Technologies) using a DNA template amplified from N2 genomic DNA (with T7 tagged primers: 5′-tgagcaacagctcaaggaga-3′ and 5′-acaaaaataggggtgggag-3′) and F1 progeny were analyzed.

Microscopy

Animals were immobilized using 0.05% tetramisole hydrochloride on 3% agar pads, imaged with a Zeiss Axio Imager Z1 equipped with a Photometrics Cool Snap HQ^2 camera, and analyzed using Metamorph software.

Analysis of Microtubule Dynamics

EBP-2::GFP dynamics were analyzed similarly as previously described (Ghosh-Roy et al., 2012). Animals were immobilized without anesthetics using a suspension of 0.1 μm polystyrene beads on 12.5% agarose pads made with M9. Live imaging was performed with a Yokogawa Confocal Scanner Unit CSU-W1 attached to a Zeiss Axio Observer and fitted with a Hamamatsu C11440-22C sCMOS camera (2,048 × 2,048, with 2 × 2 binning) and Slidebook 5.5.4 software. EBP-2::GFP dynamics were captured with 114 ms exposures captured every 230 ms for 200 frames. ImageJ 1.47u was used to generate kymographs from the initial 25 μm of the PLM axon, from which EBP-2::GFP tracks were manually traced to calculate their growth size and duration (as shown in the schematic in Figure 6A). Only tracks that were completely imaged and longer than 0.5 μm were analyzed. Catastrophe frequency represents the ratio of the total number of tracks divided by the duration of all growth events within the kymographs (Stepanova et al., 2010).

Phenotypic Analyses

Unless otherwise stated, all analyses were performed on 3-day-old adults. Axonal breaks were only classified as breaks when a distal fragment was visible; however, due to an increased rate of distal clearance in *mec-12* and *mec-7* animals, degeneration was recorded when a distal fragment was present or when the axons were significantly shorter than in wild-type animals. Light-touch assays were performed as previously described (Chalfie and Sulston, 1981). Scoring of mitochondria was performed in animals without axonal degeneration, so as to eliminate bias caused by shortening of axons in *mec-17* mutants with breaks. To determine the axonal positioning of mitochondria and accumulation of UNC-104::GFP, the axon was divided into three equal-sized segments using ImageJ 1.47u and labeled as proximal, central, and distal in relation to the cell body. UNC-104::GFP pooling at the distal end was scored when there was a clear accumulation of bright fluorescence, whereas axonal accumulation was recorded when fluorescent puncta were at least twice as bright as adjacent axon segments and when they caused the axon to at least double in width. PLM posterior outgrowth was recorded as a defect when it reached a length significantly longer than wild-type animals (greater than approximately four cell-body lengths and frequently branched), and ALM posterior outgrowth was considered a defect when the neurite was greater than two cell bodies in length. Metamorph software was used to measure body length, with the length of a central line from head to tail being recorded.

Drug Treatment

Animals were grown on nematode growth media (NGM) agar plates containing 0.1 mM colchicine (Sigma-Aldrich) or 1 μM paclitaxel (Sigma-Aldrich) in DMSO as previously described (Chalfie and Thomson, 1982; Kirszenblat et al., 2013). For control plates, animals were grown with 1% DMSO. P0 animals were grown from L4 stage on drug plates and their F1 progeny were scored.

Lifespan Analysis

Lifespan assays were conducted by transferring L4-stage animals to NGM agar plates containing 0.1 mg/ml 5-fluoro-2′-deoxyuridine (Sigma-Aldrich), which causes sterility without affecting adult morphology or lifespan (Mitchell et al., 1979). Animal viability was analyzed daily, with visualization of body movement and pharyngeal pumping providing evidence of life and prodding with a platinum wire pick used to confirm life or death in the absence of these signs.

Statistical Analysis

Statistical analyses were performed using Primer of Biostatistics 3.01 and Microsoft Excel 2011. Error of proportions was used to assess variation across a single population, and two-way comparisons were performed using the Student's t test.

SUPPLEMENTAL INFORMATION

Supplemental Information includes six figures and two movies and can be found with this article online at http://dx.doi.org/10.1016/j.celrep.2013.12.004.

ACKNOWLEDGMENTS

We thank Cori Bargmann in whose lab this project was initiated and who provided reagents; Toshihiko Oka, Sandhya Koushika, Michael Nonet, Martin Chalfie, Anindya Ghosh-Roy, Andrew Chisholm, and Jacek Gaertig for strains and reagents; Steve Zuryn, Luke Hammond, and Paula Mugno Ramirez for

technical assistance; and Rowan Tweedale, Paolo Bazzicalupo, Pankaj Sah, Kang Shen, Sean Millard, Rosina Giordano-Santini, Annika Nichols, and members of the Hilliard lab for helpful discussion and comments on the manuscript. Nematode strains used in this work were provided by the *Caenorhabditis* Genetics Center, which is funded by the National Institutes of Health (NIH) National Center for Research Resources, and the International *C. elegans* Gene Knockout Consortium. This work was supported by grants from NIH R01NS060129, National Health and Medical Research Council Project Grants 569500 and 631634, and an Australian Research Council Future Fellowship (to M.A.H.).

Received: April 25, 2013
Revised: October 31, 2013
Accepted: December 3, 2013
Published: December 26, 2013

REFERENCES

Akella, J.S., Wloga, D., Kim, J., Starostina, N.G., Lyons-Abbott, S., Morrissette, N.S., Dougan, S.T., Kipreos, E.T., and Gaertig, J. (2010). MEC-17 is an α-tubulin acetyltransferase. Nature *467*, 218–222.

Bartolini, F., Tian, G., Piehl, M., Cassimeris, L., Lewis, S.A., and Cowan, N.J. (2005). Identification of a novel tubulin-destabilizing protein related to the chaperone cofactor E. J. Cell Sci. *118*, 1197–1207.

Bommel, H., Xie, G., Rossoll, W., Wiese, S., Jablonka, S., Boehm, T., and Sendtner, M. (2002). Missense mutation in the tubulin-specific chaperone E (Tbce) gene in the mouse mutant progressive motor neuronopathy, a model of human motoneuron disease. J. Cell Biol. *159*, 563–569.

Brenner, S. (1974). The genetics of Caenorhabditis elegans. Genetics *77*, 71–94.

Cai, D., McEwen, D.P., Martens, J.R., Meyhofer, E., and Verhey, K.J. (2009). Single molecule imaging reveals differences in microtubule track selection between Kinesin motors. PLoS Biol. *7*, e1000216.

Chalfie, M., and Sulston, J. (1981). Developmental genetics of the mechanosensory neurons of *Caenorhabditis elegans*. Dev. Biol. *82*, 358–370.

Chalfie, M., and Thomson, J.N. (1982). Structural and functional diversity in the neuronal microtubules of *Caenorhabditis elegans*. J. Cell Biol. *93*, 15–23.

Coleman, M. (2005). Axon degeneration mechanisms: commonality amid diversity. Nat. Rev. Neurosci. *6*, 889–898.

Court, F.A., and Coleman, M.P. (2012). Mitochondria as a central sensor for axonal degenerative stimuli. Trends Neurosci. *35*, 364–372.

Cueva, J.G., Hsin, J., Huang, K.C., and Goodman, M.B. (2012). Posttranslational acetylation of α-tubulin constrains protofilament number in native microtubules. Curr. Biol. *22*, 1066–1074.

d'Ydewalle, C., Krishnan, J., Chiheb, D.M., Van Damme, P., Irobi, J., Kozikowski, A.P., Vanden Berghe, P., Timmerman, V., Robberecht, W., and Van Den Bosch, L. (2011). HDAC6 inhibitors reverse axonal loss in a mouse model of mutant HSPB1-induced Charcot-Marie-Tooth disease. Nat. Med. *17*, 968–974.

Davis, M.W., Hammarlund, M., Harrach, T., Hullett, P., Olsen, S., and Jorgensen, E.M. (2005). Rapid single nucleotide polymorphism mapping in *C. elegans*. BMC Genomics *6*, 118.

Desai, A., and Mitchison, T.J. (1997). Microtubule polymerization dynamics. Annu. Rev. Cell Dev. Biol. *13*, 83–117.

Dompierre, J.P., Godin, J.D., Charrin, B.C., Cordelières, F.P., King, S.J., Humbert, S., and Saudou, F. (2007). Histone deacetylase 6 inhibition compensates for the transport deficit in Huntington's disease by increasing tubulin acetylation. J. Neurosci. *27*, 3571–3583.

Falnikar, A., and Baas, P.W. (2009). Critical roles for microtubules in axonal development and disease. Results Probl. Cell Differ. *48*, 47–64.

Fojo, T. (2008). The Role of Microtubules in Cell Biology, Neurobiology, and Oncology (Totowa, NJ: Humana Press).

Gardiner, J., Barton, D., Marc, J., and Overall, R. (2007). Potential role of tubulin acetylation and microtubule-based protein trafficking in familial dysautonomia. Traffic *8*, 1145–1149.

Ghosh-Roy, A., Goncharov, A., Jin, Y., and Chisholm, A.D. (2012). Kinesin-13 and tubulin posttranslational modifications regulate microtubule growth in axon regeneration. Dev. Cell *23*, 716–728.

Gumienny, T.L., MacNeil, L.T., Wang, H., de Bono, M., Wrana, J.L., and Padgett, R.W. (2007). Glypican LON-2 is a conserved negative regulator of BMP-like signaling in *Caenorhabditis elegans*. Curr. Biol. *17*, 159–164.

Hall, D.H., and Hedgecock, E.M. (1991). Kinesin-related gene *unc-104* is required for axonal transport of synaptic vesicles in *C. elegans*. Cell *65*, 837–847.

Hammond, J.W., Cai, D., and Verhey, K.J. (2008). Tubulin modifications and their cellular functions. Curr. Opin. Cell Biol. *20*, 71–76.

Hammond, J.W., Huang, C.F., Kaech, S., Jacobson, C., Banker, G., and Verhey, K.J. (2010). Posttranslational modifications of tubulin and the polarized transport of kinesin-1 in neurons. Mol. Biol. Cell *21*, 572–583.

Hempen, B., and Brion, J.P. (1996). Reduction of acetylated α-tubulin immunoreactivity in neurofibrillary tangle-bearing neurons in Alzheimer's disease. J. Neuropathol. Exp. Neurol. *55*, 964–972.

Hilliard, M.A. (2009). Axonal degeneration and regeneration: a mechanistic tug-of-war. J. Neurochem. *108*, 23–32.

Hollenbeck, P.J. (1996). The pattern and mechanism of mitochondrial transport in axons. Front. Biosci. *1*, d91–d102.

Ichishita, R., Tanaka, K., Sugiura, Y., Sayano, T., Mihara, K., and Oka, T. (2008). An RNAi screen for mitochondrial proteins required to maintain the morphology of the organelle in *Caenorhabditis elegans*. J. Biochem. *143*, 449–454.

Janke, C., and Bulinski, J.C. (2011). Post-translational regulation of the microtubule cytoskeleton: mechanisms and functions. Nat. Rev. Mol. Cell Biol. *12*, 773–786.

Kalebic, N., Martinez, C., Perlas, E., Hublitz, P., Bilbao-Cortes, D., Fiedorczuk, K., Andolfo, A., and Heppenstall, P.A. (2013a). Tubulin acetyltransferase αTAT1 destabilizes microtubules independently of its acetylation activity. Mol. Cell. Biol. *33*, 1114–1123.

Kalebic, N., Sorrentino, S., Perlas, E., Bolasco, G., Martinez, C., and Heppenstall, P.A. (2013b). αTAT1 is the major α-tubulin acetyltransferase in mice. Nat. Commun. *4*, 1962.

Kanaji, S., Iwahashi, J., Kida, Y., Sakaguchi, M., and Mihara, K. (2000). Characterization of the signal that directs Tom20 to the mitochondrial outer membrane. J. Cell Biol. *151*, 277–288.

Kenyon, C., Chang, J., Gensch, E., Rudner, A., and Tabtiang, R. (1993). A *C. elegans* mutant that lives twice as long as wild type. Nature *366*, 461–464.

Kirszenblat, L., Neumann, B., Coakley, S., and Hilliard, M.A. (2013). A dominant mutation in *mec-7/β-tubulin* affects axon development and regeneration in *Caenorhabditis elegans* neurons. Mol. Biol. Cell *24*, 285–296.

Konishi, Y., and Setou, M. (2009). Tubulin tyrosination navigates the kinesin-1 motor domain to axons. Nat. Neurosci. *12*, 559–567.

Krishna, S., Maduzia, L.L., and Padgett, R.W. (1999). Specificity of TGFbeta signaling is conferred by distinct type I receptors and their associated SMAD proteins in Caenorhabditis elegans. Development *126*, 251–260.

Kumar, J., Choudhary, B.C., Metpally, R., Zheng, Q., Nonet, M.L., Ramanathan, S., Klopfenstein, D.R., and Koushika, S.P. (2010). The *Caenorhabditis elegans* Kinesin-3 motor UNC-104/KIF1A is degraded upon loss of specific binding to cargo. PLoS Genet. *6*, e1001200.

L'Hernault, S.W., and Rosenbaum, J.L. (1985). *Chlamydomonas* α-tubulin is posttranslationally modified by acetylation on the ε-amino group of a lysine. Biochemistry *24*, 473–478.

MacLeod, A.R., Waterston, R.H., Fishpool, R.M., and Brenner, S. (1977). Identification of the structural gene for a myosin heavy-chain in *Caenorhabditis elegans*. J. Mol. Biol. *114*, 133–140.

Martin, L.J. (2012). Biology of mitochondria in neurodegenerative diseases. Prog. Mol. Biol. Transl. Sci. *107*, 355–415.

Mitchell, D.H., Stiles, J.W., Santelli, J., and Sanadi, D.R. (1979). Synchronous growth and aging of *Caenorhabditis elegans* in the presence of fluorodeoxyuridine. J. Gerontol. *34*, 28–36.

Morita, K., Flemming, A.J., Sugihara, Y., Mochii, M., Suzuki, Y., Yoshida, S., Wood, W.B., Kohara, Y., Leroi, A.M., and Ueno, N. (2002). A *Caenorhabditis elegans* TGF-β, DBL-1, controls the expression of LON-1, a PR-related protein, that regulates polyploidization and body length. EMBO J. *21*, 1063–1073.

Nogales, E., Wolf, S.G., and Downing, K.H. (1998). Structure of the α β tubulin dimer by electron crystallography. Nature *391*, 199–203.

Nonet, M.L., Staunton, J.E., Kilgard, M.P., Fergestad, T., Hartwieg, E., Horvitz, H.R., Jorgensen, E.M., and Meyer, B.J. (1997). *Caenorhabditis elegans rab-3* mutant synapses exhibit impaired function and are partially depleted of vesicles. J. Neurosci. *17*, 8061–8073.

Nyström, J., Shen, Z.Z., Aili, M., Flemming, A.J., Leroi, A., and Tuck, S. (2002). Increased or decreased levels of *Caenorhabditis elegans lon-3*, a gene encoding a collagen, cause reciprocal changes in body length. Genetics *161*, 83–97.

Perdiz, D., Mackeh, R., Poüs, C., and Baillet, A. (2011). The ins and outs of tubulin acetylation: more than just a post-translational modification? Cell. Signal. *23*, 763–771.

Raff, M.C., Whitmore, A.V., and Finn, J.T. (2002). Axonal self-destruction and neurodegeneration. Science *296*, 868–871.

Reed, N.A., Cai, D., Blasius, T.L., Jih, G.T., Meyhofer, E., Gaertig, J., and Verhey, K.J. (2006). Microtubule acetylation promotes kinesin-1 binding and transport. Curr. Biol. *16*, 2166–2172.

Savage, C., Das, P., Finelli, A.L., Townsend, S.R., Sun, C.Y., Baird, S.E., and Padgett, R.W. (1996). *Caenorhabditis elegans* genes *sma-2, sma-3*, and *sma-4* define a conserved family of transforming growth factor β pathway components. Proc. Natl. Acad. Sci. USA *93*, 790–794.

Savage-Dunn, C., Tokarz, R., Wang, H., Cohen, S., Giannikas, C., and Padgett, R.W. (2000). SMA-3 smad has specific and critical functions in DBL-1/SMA-6 TGFbeta-related signaling. Dev. Biol. *223*, 70–76.

Shida, T., Cueva, J.G., Xu, Z., Goodman, M.B., and Nachury, M.V. (2010). The major α-tubulin K40 acetyltransferase alphaTAT1 promotes rapid ciliogenesis and efficient mechanosensation. Proc. Natl. Acad. Sci. USA *107*, 21517–21522.

Soete, G., Betist, M.C., and Korswagen, H.C. (2007). Regulation of *Caenorhabditis elegans* body size and male tail development by the novel gene *lon-8*. BMC Dev. Biol. *7*, 20.

Srayko, M., Kaya, A., Stamford, J., and Hyman, A.A. (2005). Identification and characterization of factors required for microtubule growth and nucleation in the early *C. elegans* embryo. Dev. Cell *9*, 223–236.

Stepanova, T., Smal, I., van Haren, J., Akinci, U., Liu, Z., Miedema, M., Limpens, R., van Ham, M., van der Reijden, M., Poot, R., et al. (2010). History-dependent catastrophes regulate axonal microtubule behavior. Curr. Biol. *20*, 1023–1028.

Suzuki, Y., Yandell, M.D., Roy, P.J., Krishna, S., Savage-Dunn, C., Ross, R.M., Padgett, R.W., and Wood, W.B. (1999). A BMP homolog acts as a dose-dependent regulator of body size and male tail patterning in *Caenorhabditis elegans*. Development *126*, 241–250.

Topalidou, I., Keller, C., Kalebic, N., Nguyen, K.C., Somhegyi, H., Politi, K.A., Heppenstall, P., Hall, D.H., and Chalfie, M. (2012). Genetically separable functions of the MEC-17 tubulin acetyltransferase affect microtubule organization. Curr. Biol. *22*, 1057–1065.

Wang, J.T., Medress, Z.A., and Barres, B.A. (2012). Axon degeneration: molecular mechanisms of a self-destruction pathway. J. Cell Biol. *196*, 7–18.

Westermann, S., and Weber, K. (2003). Post-translational modifications regulate microtubule function. Nat. Rev. Mol. Cell Biol. *4*, 938–947.

Wicks, S.R., Yeh, R.T., Gish, W.R., Waterston, R.H., and Plasterk, R.H. (2001). Rapid gene mapping in *Caenorhabditis elegans* using a high density polymorphism map. Nat. Genet. *28*, 160–164.

Zhang, Y., Ma, C., Delohery, T., Nasipak, B., Foat, B.C., Bounoutas, A., Bussemaker, H.J., Kim, S.K., and Chalfie, M. (2002). Identification of genes expressed in *C. elegans* touch receptor neurons. Nature *418*, 331–335.

Zuryn, S., Le Gras, S., Jamet, K., and Jarriault, S. (2010). A strategy for direct mapping and identification of mutations by whole-genome sequencing. Genetics *186*, 427–430.